Colloid and Polymer Science (2021) 299:1595–1603
https://doi.org/10.1007/s00396-021-04893-8

ORIGINAL CONTRIBUTION

Rotational and translational diffusion of colloidal ellipsoids in bulk and at surfaces

Namita Shokeen[1] · **Ashis Mukhopadhyay**[1]

Received: 21 April 2021 / Revised: 18 August 2021 / Accepted: 20 August 2021 / Published online: 31 August 2021

Abstract

We studied the diffusion of ellipsoidal colloids by using a combination of single-particle tracking (SPT) and differential dynamic microscopy (DDM). The micrometer-sized polystyrene particles have an aspect ratio of ≈ 4.3. SPT provides the particle trajectories and translation diffusion coefficient of the particles. DDM analyses appropriate for anisotropic particles were then used to extract the rotational diffusion coefficient of the particles. The results matched well with the theoretical prediction of translational and rotational diffusion coefficients for ellipsoids in the bulk. We extended our method to surface bound particles, which shows that rotation slowed by a larger amount compared to translation. This can be explained qualitatively by assuming heterogeneity of viscous and hydrodynamic forces experienced by surface bound particles. The research will be useful to study the viscous friction experienced by anisotropic colloids in complex fluids and surface friction at chemically or topologically modified substrates.

Keywords Rotational diffusion · Translational diffusion · Anisotropic colloids · Differential dynamic microscopy · Single-particle tracking

Introduction

The studies of translational and rotational dynamics of anisotropic colloids are important both for fundamental physics and because of the use of these colloids for various applications. Anisotropy is very common for biological systems as many biomolecules such as DNA, proteins (e.g., keratin), and viruses (e.g., tobacco mosaic virus) are anisotropic. Anisotropic particles (e.g., carbon nanotubes) are also widely used to make high-performance polymer composites, which find various applications in technology and manufacturing. From fundamental physics point of view, the studies help to verify or refute various theories and simulations aimed towards describing the motion of these particles. In contrast to the isotropic spherical particles, experimental methods available for synthesizing and characterizing the dynamics of anisotropic colloids are overall limited. The techniques, such as depolarized dynamic light scattering (d-DLS) [1–3], confocal laser scanning microscopy (CLSM) [4], fluorescence correlation spectroscopy (FCS) [5], and fluorescence recovery after photobleaching (FRAP) [6], have contributed to understanding the motion of some anisotropic particles, such as rods.

Among some of the most relevant experiments, Han et al. measured the rotational Brownian motions of single ellipsoids in a quasi-two-dimensional confinements by using video microscopy [4]. They measured both the short-time anisotropic and long-time isotropic rotational diffusion along the major and minor axes of ellipsoids. The coupling between rotation and translation changed the anisotropy of translational diffusion at short-length scale to isotropic diffusion at long-time scales. The cross-over time is determined by the inverse of the rotational diffusion coefficient. They found that confinement in two dimensions alters the diffusion anisotropy (the ratio of the diffusion coefficient along the major to the minor axes) and the diffusion along the minor axis is much slower than the bulk diffusion in three dimensions. Cush et al. used depolarized dynamic light scattering to determine the translational as well as rotational diffusion of tobacco mosaic virus (TMV) within aqueous polymer solutions of flexible carbohydrate dextran (M_W ~ 505,000) [3]. TMV can be approximated as a very long and thin cylinder with a high aspect ratio. The goal was

✉ Ashis Mukhopadhyay
ashis@wayne.edu

[1] Department of Physics, Wayne State University, Detroit, MI 48201, USA

to compare the measured diffusion coefficients in solutions of polymer of various architecture with continuum theory prediction. TMV in solution was also used to measure the anisotropy of diffusion and as a model system of particles with very high aspect ratio for comparison with hydrodynamic theories [7]. The experiments observed that apparent diffusion coefficient (D_{app}) which is determined by contributions from center-of-mass diffusion, anisotropy, and rotation of the particles depends upon wave vector (q). D_{app} reaches a plateau value that is independent of q for $qL >> 1$, where L is the length of the rod. Alam et al. investigated translational and rotational diffusion of gold nanorods within various entangled solutions of polyethylene glycol (PEG) solutions with different molecular weights. They used multi-photon fluctuation correlation spectroscopy (FCS) to calculate the nanoviscosity experienced by nanorods within different PEG concentrations [8]. The results were compared to different theories. FCS was also used for studying quantum nanorods' (NRs) diffusion and its dependence on aspect ratios by Tsay et al. Rotational diffusion was found to be more sensitive to change in rods' sizes and occurring at faster time scales than the translational diffusion as predicted in different theories [5]. They extended their studies to investigate the non-specific binding of peptide-coated NRs with bovine serum albumin (BSA) by titrating and reported that rotational diffusion coefficient can be used as a probe to study the effects of binding and conformational change of macromolecules.

Many recent advances in synthetic methods made possible studies of particles possessing lower symmetry compared to ellipsoids or rod-like particles. Anthony et al. used single-particle tracking to study diffusion of particle clusters of different shapes and sizes in a quasi-two-dimensional (2D) geometry [9]. The clusters were made starting from silica spheres jointed with each other by a thin film of silica. They found that the effective hydrodynamic radius, as measured by the translation and rotation of the clusters, differed significantly. It indicated that the Stokes–Einstein-Debye (SED) relation that couples the translational and rotational diffusion of spherical particles cannot be applied in a straightforward manner to anisotropic particle clusters. Stuckert et al. had also studied particle clusters, but their synthesis protocol using emulsion technique produced particles that are deformed and partially fused with neighboring particles [10]. For dense particle clusters with a relatively small aspect ratio (tetrahedrons and octahedrons), they observed that $D_{tran} \sim 1/R$ and $D_{rot} \sim 1/R^3$, which is in accord to the SED relation. Here, D_{tran} and D_{rot} are translational and rotational diffusion coefficients, respectively, and R is the particle radius. Significant deviation from SED theory was observed for clusters possessing higher aspect ratio (doublets, triplets, and triangular dipyramids). Chakrabarty et al. studied the diffusion of Boomerang-shaped particles in a quasi-2D geometry [11]. For such asymmetric particles, they pointed out the significance of the center of hydrodynamic stress (CoH). Their results showed that motion of a tracking point is a superposition of two independent diffusive modes: the ellipsoidal motion of the CoH and the rotational motion of the individual points on the particle about the CoH.

Compared to many experimental techniques, in particular depolarized dynamic light scattering (d-DLS), which is commonly used to characterize anisotropic particles, DDM has several advantages [12]. It is cost-effective and does not require coherent light sources, sophisticated detectors, optics, and electronics. It needs a very small amount of sample and can function in concentrated solutions. The latter can be an issue in d-DLS due to multiple scattering problem, where alternate methods, such as diffusive wave spectroscopy, need to be used. The scattering-based methods are also more suitable for studies in bulk [13]. DDM and DLS are complementary in terms of length scale and time scale of experiments. DDM is the preferred technique to probe the small wave-vector range at a longer time scale compared to DLS. Here, we report a quick method to determine the ensemble averaged translational and rotational diffusion coefficients of ellipsoids by using a combination of single-particle tracking (SPT) and differential dynamic microscopy (DDM).

DDM, a relatively new method, provides the dynamical information of particles in the reciprocal space that can use a broad range of video microscopic techniques, commonly available in all laboratories [12, 14–17]. In reciprocal space, DDM provides dynamical information in the form of characteristic time scales for a range of wave vectors that complements DLS method. There are a couple of studies of using DDM that are pertinent to this work. Reufer et al. measured the translational diffusion of spindle-shaped hematite particles in the presence of external magnetic field [18]. They determined the anisotropy of diffusion, $D_{\parallel}$ and $D_{\perp}$, where the direction is set by magnetic field orientation. Here, $D_{\parallel}$ ($D_{\perp}$) is diffusion coefficient parallel (perpendicular) to the magnetic field. DDM was also used to study rotational diffusion of substrate bound Janus particles [19]. Here, the particles' translational diffusion is quenched, but they can still rotate. They extended their method to the limit of single particles and studied both rotational diffusion and constant rotational motion.

Pal et al. recently studied anisotropic diffusion of ellipsoidal particles possessing a magnetic core by using DDM [20]. The diffusion anisotropy originated from an external magnetic field, which defines a preferred direction of orientation of the particles. The anisotropy of diffusion increases with the strength of the magnetic field. They extended the use of DDM to the concentration regime approaching the glass transition in three dimensions, where traditional technique such as the single-particle tracking and d-DLS

becomes difficult. Their data suggested that kinetic arrest near the transition is related to the formation of nearest neighbor cages as in glasses formed by hard spheres and is independent of whether an aligning field was present was not. However, the cage dynamics is affected by the strength of the field. They did not observe the type of glass formed by the creation of nematic domains in the presence of the field. The authors did not study how the rotational diffusion of the ellipsoids is affected on approach to the glass transition, which is one of the objectives of this work.

Here, we combined single-particle tracking with DDM to probe rotational diffusion and long-time translational diffusion of ellipsoidal colloids. The particle tracking was used to determine the translation diffusion coefficient (D_t) of the center of mass of colloidal ellipsoids. After validating our results with theoretical prediction of diffusion coefficients in the bulk, we extended our method in situations, where the ellipsoids are confined near a surface. Here, both rotational and translational motions are quenched due to additional friction between the substrate (coverslip) and the particles. The method outlined here provides an opportunity to measure the friction coefficients in a relatively straightforward manner.

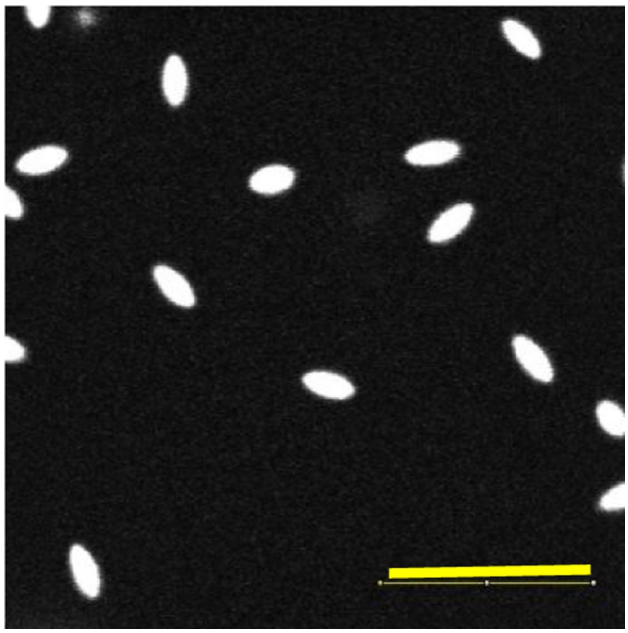

Fig. 1 Microscopy images of ellipsoids formed by the method described earlier. The scale bars are 10 μm

Experimental section

Microellipsoids were synthesized starting from 1 μm diameter fluorescently labeled polystyrene (PS) spheres (Thermo Fisher, Inc.). The spheres were embedded in an elastomeric film of poly(dimethyl siloxane) (PDMS). This material is clamped, heated above the glass transition temperature of the matrix (≈ 130 °C), and then a uniaxial elongation was carried out by continuous stretching [21]. The aspect ratio, $r = \frac{a}{b}$, where $2a$ is the length and $2b$ is the width of the ellipsoids, depends on the amount of strain (Fig. 1). Using the analysis of confocal microscopy images, we determined that $2a = 2.6 \pm 0.3$ μm, and by using conservation of volume, we determined, $2b \approx 0.6 \pm 0.08$ μm, which gives the aspect ratio ≈ 4.3. The histogram of size distribution of the major axis of the ellipsoids is shown in Supplementary Materials 1. The standard deviation for the minor axis was calculated by assuming that PS spheres have a polydispersity of 10% according to the manufacturer specification. The microellipsoids were suspended in deionized water at a volume fraction of less than 0.01. About 10 μl of the sample volumes were loaded on $3'' \times 1'' \times 1.0$ mm sized plain beveled edge microscope slides, which were covered with a thin cover glass on top with a double-sided scotch tape that acts as a spacer. The assembly was sealed at the edges to prevent evaporation. In addition to freely diffusing colloids, at a few locations, we observed ellipsoids loosely but irreversibly attached to the surface of the coverslips. These particles exhibited different translational and rotational diffusions compared to bulk. These particles were used to determine the surface friction coefficients. The movies were collected by using an optical microscope (inverted Nikon A1Rsi) with an oil objective (N. A. = 1.4, 100×) and a fast ccd camera.

Particle tracking analysis was carried out by using u-track, a SPT algorithm developed by Danuser laboratory [22] with some modifications by us to calculate the mean-square-displacement. We verified the measurements of translational diffusion by SPT with differential dynamic analysis. Briefly, DDM analysis consists of following few steps [12, 18, 19]. Each sample image in the video represents a spatial light intensity distribution I (x,y,t) at some time t. A difference image signal ΔI (x,y,Δt) was calculated by subtracting one image from another for each image pair present in the video. This step gets rid of all intensity signals that are unnecessary for our purpose, i.e., static noise contributions and non-motile signals coming from particles stuck on microscope slides or dust on optics. In order to get dynamical information in reciprocal space, a fast Fourier transform ΔI (q_x,q_y,Δt) of each difference signal ΔI (x, y,Δt) can be calculated which gives us a Fourier distribution of intensity fluctuations for each difference signal. A statistical averaging of ΔI (q_x,q_y,Δt) over all image pairs provides us a 2D ensemble averaged distribution given by $< \Delta I\,(q_x,q_y,\Delta t) >$. Finally, the image structure function D (q_x,q_y,Δt) can be calculated from the two-dimensional power spectra in Fourier space in the form of $<|\Delta I(q_x,q_y,\Delta t)|^2>$. As there is no preferred direction, we can use the radially averaged image structure

$D(q, \Delta t)$ function is given by $D(q, \Delta t) = <|\Delta I(q, \Delta t)|^2>$, where the wave vector (q) is calculated by $q = (q_x^2 + q_y^2)^{½}$. The whole process is repeated for many time steps in the image stack. Finally, the image structure function for processes involving single relaxation with characteristic time τ is fitted to the equation as [12]:

$$D(q, \Delta t) = A(q)\left[1 - exp\left(\frac{-\Delta t}{\tau(q)}\right)\right] + B(q)$$

where $A(q)$ is the convolution of the particles' scattering properties with the optical transfer function of the imaging optics and $B(q)$ is related to the imaging noise and incoherent scattering.

Results and discussion

First, we determine the centroid locations of the ellipsoids using Image J. This has an uncertainty of about 40 nm. A Gaussian filter was used and a specified noise was added. We determined that the last two steps were needed to run the u-track program, which gives the trajectories of the particles (Supplementary Materials, 2). The displacement of the particles in one specific direction ($-x$) as a function of time is shown in Fig. 2a. Perrin et al. have shown that $<D_x> = <D_y> = D$ based upon dynamic light scattering experiments [13]. From particle trajectories, we determined the probability density functions at different times, which show the Gaussian distribution of displacement (Fig. 2b). The mean-square-displacement (MSD) of the particle depends linearly on time lag as in normal Brownian motion (Fig. 2c). The latter was then analyzed to determine the ensemble averaged translation diffusion coefficient, D_t. In bulk, we determine $D_t \approx 0.4 \pm 0.03$ μm^2/s, where the ± indicates the fitting error of Fig. 2c.

The translation diffusion is expected to be anisotropic for time scale (τ_r) less than $1/(6D_r)$ in the bulk, where D_r is the rotational diffusion coefficient[4]. Much below τ_r, one expects two distinct translation diffusion coefficients for an anisotropic particle—one parallel to the major axis and the other perpendicular to it. Much above τ_r, one will measure a single rotationally averaged translational diffusion coefficient. The diffusion coefficient along the major axis (D_a) of the ellipsoids is higher compared to diffusion coefficient along the minor axis (D_b). The ratio, D_a/D_b, increases from 1 to 2 with the increase of the aspect ratio (a/b) of the particles [4, 23]. Experimentally, for very thin rods, such as tobacco mosaic virus (TMV), the ratio D_a/D_b can reach a value close to 2 [7]. The prediction applies only when the particles are freely diffusing in bulk. At surfaces and under confinement, D_a/D_b can assume a much larger value [4]. From our experiments as well as from theoretical estimates, we determined that $\tau_r \approx 0.5$ s in the bulk as $D_r \approx 0.4$ s. We can, therefore, expect two different translational diffusion coefficients for time below ≈ 0.5 s. The contribution of the diffusion anisotropy, which is defined as $\Delta = D_a - D_b$ to the measured apparent diffusion coefficient (D_{app}), will be discussed later.

In Fig. 3a, we show the image structure function obtained from DDM analysis for some selective wave vectors, in situations where ellipsoids are moving freely in three dimensions. The curves were fitted with a single exponential function, from which q-dependent relaxation times were obtained. It has been shown recently that the abrupt cut-off of the finite-size image causes spurious high-frequency artifacts in DDM analysis [24]. Specifically, a regime of wave-vector independent relaxation time is obtained at higher q. It can be eliminated by applying a window function in the original image. In all our analyses, we employed a Hann windowing function before performing the DDM analysis [24]. The effect of applying the window function is shown in Fig. S3.

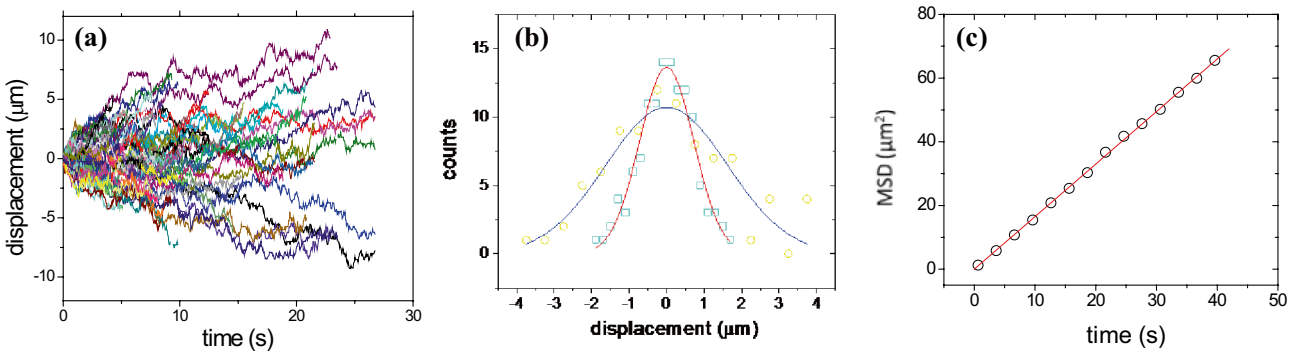

Fig. 2 (**a**) The displacement of ellipsoids in x-direction as a function of time in the bulk. (**b**) The distribution of displacement at times $t = 0.66$ s (squares), $t = 3.33$ s (circles) and fitted with Gaussian functions. (**c**) The mean square displacement (MSD) as a function of time (t) with straight line of slope 1.6 μm^2/s, which gives rotationally averaged $D_t \approx 0.4$ μm^2/s

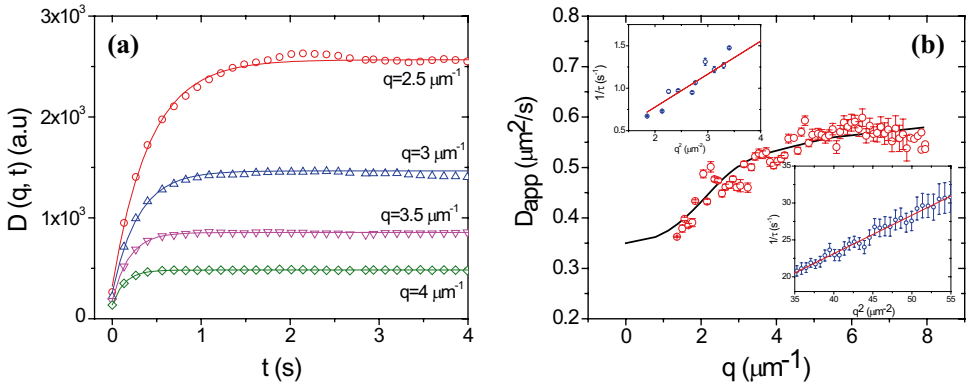

Fig. 3 (**a**) The image structure functions vs. time interval for four different values of wave vectors for the microellipsoids diffusing freely in water. The solid lines correspond to the fittings of image structure function assuming a single exponential relaxation. (**b**) The apparent diffusion coefficient, D_{app} plotted against q. The solid-line fitting is with the model as described in the text. The upper inset shows the plot of $1/\tau$ vs. q^2 for small wave vectors, which gives translational diffusion coefficient. The lower inset is the same plot for higher wave vectors, which has a higher slope that gives the sum of translational and rotational diffusion coefficients

For homogeneous spherical particles, the wave-vector dependent relaxation time is given by, $\tau(q) = 1/D_{s,\text{tsran}}q^2$. In Fig. S4a, we have shown the plot of $1/\tau(q)$ vs. q^2 for 1 μm polystyrene particles diffusing freely in water for $0.67\ \mu m^{-1} < q < 7.1\ \mu m^{-1}$. The fitting of the data with a straight line passing through origin gives, $D_t \approx 0.45 \pm 0.015\ \mu m^2/s$, which is in good agreement with the expectation from Stokes–Einstein (SE) relation. For anisotropic particles, the rotational diffusion also contributes to the relaxation time so that its q-dependence can be written as $\tau(q) = 1/(D_t q^2 + 6D_r)$, where D_t is rotationally averaged translational diffusion coefficient as given by [18, 25, 26]: $D_t = (D_a + 2D_b)/3$ and D_r is the rotational diffusion coefficient. A plot of $1/\tau(q)$ vs. q^2 thus will give a slope of D_t and an intercept of $6D_r$. However, extracting D_r from the intercept in this manner is difficult as we observed that even for spherical particles a graph of $1/\tau(q)$ vs. q^2 yields a small but non-zero intercept when the linear regression is performed without any constraints. A different analysis procedure is thus needed.

In scattering experiments for high aspect ratio rods and in the small wave-vector limit of $qL << 1$, where $L = 2a$ is the length of the rod, one experimentally measures the rotationally averaged translational diffusion coefficient D_t [2, 3, 7]. The rotation of the particles and anisotropy of translation diffusion (Δ) do not contribute to the image structure function and in the relaxation time in this limit. At higher values of the wave vectors, in addition to D_t, both anisotropy and rotation contribute, and the measured diffusion coefficient becomes wave-vector dependent. For thin and long rods, in the large wave-vector limit of $qL >> 1$, the apparent diffusion coefficient slowly reaches a plateau independent of q [27]. The apparent diffusion coefficient is given by $D_{app} = D_t - \Delta/3 + L^2 D_r/12$. The wave-vector dependent apparent diffusion coefficient can be obtained by using the relation: $D_{app} = 1/q^2\tau$, where τ is obtained by fitting the image structure function. For homogeneous spherical particles, the apparent diffusion coefficient will be wave-vector independent, and only the center of mass diffusion will contribute. To verify that, we have shown in Fig. S4b that D_{app} as a function of q^2 for 1-μm spheres diffused freely in water. The graph is close to a horizontal straight line with a slight increase at lower q values.

For ellipsoids in the bulk, the plot of D_{app} vs. q is shown in Fig. 3b, which shows deviation from the straight line. The full q-dependence of D_{app} for anisotropic particles, except for extremely high aspect ratio rods, is currently not known to the best of our knowledge. Wilcoxon *et. al.* analytically derived an expression valid for all wave vectors, which is given by $D_{app} = D_t + 2\Delta(1/3 - F(qL)) + 2L^2 D_r G(qL)$. $F(qL)$ and $G(qL)$ are universal functions with the properties of $\lim_{qL\to 0} F = \frac{1}{3}$. $\lim_{qL\to} F = \frac{1}{2}$, $\lim_{qL\to 0} G = 0$; $\lim_{qL\to} G = \frac{1}{24}$ [7]. By using the stick theory for ellipsoids, we calculated, $D_a \approx 0.48\ \mu m^2/s$, $D_b \approx 0.37\ \mu m^2/s$, $D_t = (D_a + 2D_b)/3 \approx 0.4\ \mu m^2/s$, and $\Delta \approx 0.1\ \mu m^2/s$. The contribution of anisotropy to D_{app} according to the theory, therefore, ranges from 0 at low q to a negative contribution of -0.02 at large q. The above calculation indicates a small contribution of anisotropy to apparent diffusion coefficient.

In Fig. 3b, the experimental data of D_{app} are fitted with D_t and D_r to obtain the lowest χ^2 value, which gives $D_t \approx 0.35\ \mu m^2/s$ and $D_r \approx 0.4\ s^{-1}$. The translational diffusion coefficient matches well with measurement using particle tracking, justifying our analysis method. It is customary to represent data by a plot of $1/\tau(q)$ vs. q^2, which we showed in Fig. 3b (inset) in the small wave-vector limit. The fitting of the data shows a straight line with zero intercept

Table 1 Theoretical predictions and experimental values for translational and rotational diffusion coefficients of ellipsoids in water

	Stick	TT	Boersma	Brenner	DDM	Particle tracking
D_t (μm^2/s)	0.4	0.34	0.27	0.36	0.35	0.4
D_r (s^{-1})	0.12	0.24	0.21	0.35	0.4	N.A

consistent with the translational diffusion. The slope of the line gives $D_t = 0.38 \pm 0.015$ μm^2/s (Fig. 3b). In addition, at large wave-vector range, we obtained a different and higher slope of $D_{app} \approx 0.55 \pm 0.02$ μm^2/s, which in addition to translational diffusion has contribution from rotational diffusion.

We will now compare our experimental results with the prevailing theories. Depending on the shape anisotropy, three models can be used to find the translational and rotational diffusion coefficients. They are called hydrodynamic stick (HS) theory [28], Tirado and Garcia de la Torre's (TT) theory [29], and Broersma's relations [5, 30]. TT and HS theories are applicable to rod-shaped particles of all aspect ratios, but Broersma's relation is only suitable for rods with aspect ratio greater than 3.5. There is an exact theory by Brenner [31], which for ellipsoids gave $D_a = 0.43$ (μm^2/s), $D_b = 0.33$ (μm^2/s), the rotationally averaged translational diffusion coefficient, $D_t = 0.36$ (μm^2/s), and $D_r = 0.35$ s^{-1}. The details about these models and theory have been included in Supplementary Materials. Table 1 summarizes the prediction from various theories along with the results from our experiments.

The stick theory is applicable for ellipsoids, but previous computer simulations showed that it could not explain the diffusion of either prolate or oblate spheroids [32]. This is also evident for rotational diffusion, where the stick theory predicts significantly lower value compared to experimental results. The prediction from TT theory for both translation and rotation fall below compared to experiment, but both these theories are applicable for rods and not for prolate spheroids. We also need to consider the effect of particle polydispersity and slight error in measuring the length of the ellipsoids, which can cause a large change in theoretical values. For example, if the length of the rod is taken as 2.35 μm, which is one sigma (standard deviation) value smaller than the average, TT theory predicts $D_t = 0.37$ μm^2/s and $D_r = 0.31$ s^{-1}. Our measurements by DDM agreed very well with Brenner's theory as shown in Table 1.

The methodology that we applied here can be extended to measure the diffusion coefficients and hence the friction coefficients at the solid–liquid interface. A handful of ellipsoids were found to be irreversibly but weakly attached to the glass surfaces. It can happen when the detachment energy from the surface much exceeds the thermal energy. It can still have residual surface bound motion; e.g., one can envision that particles are sitting atop of an ultra-thin layer of water, which can significantly quench their motion. Alternatively, the heterogeneity can arise from the roughness at the surface of the coverslip and particles, which can alter the local friction coefficient. These particles can rotate with their major axis parallel to the surface. As in bulk studies, we first used particle tracking to confirm that it gives similar result for D_t with DDM. As evident from particle trajectories (Supplementary

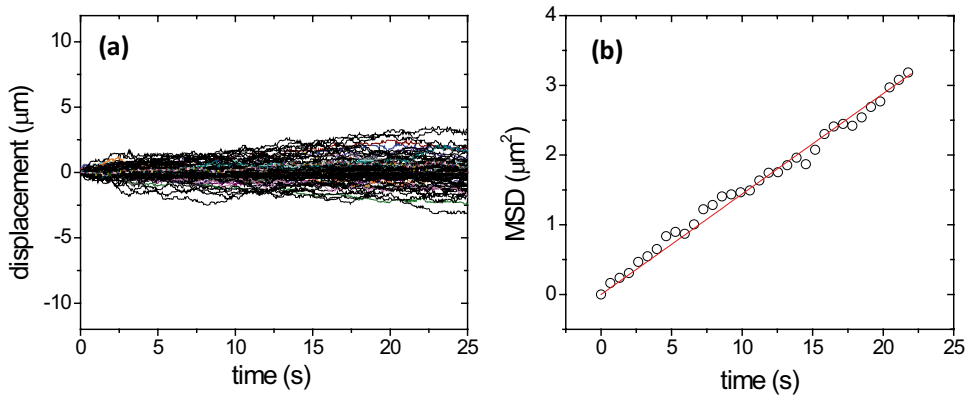

Fig. 4 (**a**) The displacement of ellipsoids in x-direction as a function of time at glass surface. Comparison with Fig. 2a shows slower diffusion of the particle due to hydrodynamic or topographical interaction with the solid substrate. The symmetric distribution of particle displacement from $x = 0$ indicates there is no directed flow. (**b**)The mean-square-displacement of an ensemble of particles plotted as a function of time. The solid line is a straight line fit with zero intercept and slope of 0.14 μm^2/s

Materials 2) at the surface and comparing the distribution of displacements (Figs. 2a, and 4a), it can be concluded that particle translational motion is significantly hindered. The plot of mean-square-displacement vs. time is a straight line with a slope of 0.14 ± 0.01 (Fig. 4b), which gives the diffusion coefficient at the surface, $D_{t,s} = 0.035 \pm 0.003$ μm^2/s.

In Fig. 5, we show the apparent diffusion coefficient, D_{app} vs. q, which showed a slow increase as observed in bulk studies. At the long wavelength limit, as D_{app} is determined by the translational part, and ignoring the anisotropy contribution, we get, $D_{t,s} \approx 0.03$ μm^2/s, which indicates a factor of ≈ 11 slow down compared to the bulk. The rotational diffusion coefficient at the surface as obtained by fitting gives $D_{r,s} \approx 0.025$ s^{-1}, which shows a factor of ≈ 16 slowing down compared to the bulk. To calculate the friction coefficient of the surface, we can use Einstein relation of fluctuation–dissipation theorem, $D = k_B T/\zeta$, where k_B is the Boltzmann constant, T is the absolute temperature, and ζ is the friction coefficient. We obtained the average friction coefficient for translation at the surface is, $\zeta_t \approx 1.6 \times 10^{-7}$ N.s/m and rotation, $\zeta_r \approx 1.62 \times 10^{-19}$ J.s by taking the temperature as $T = 296$ K.

Our results showed different slowing down of translational and rotational diffusion at the solid–liquid interface compared to the bulk. The polystyrene particles are negatively charged due to coating by carboxylic acid groups. They are well separated (more than a few microns) both at the surface and in the bulk so that the particle–particle interaction can be safely neglected. We used deionized water, but the release of ions from the glass surface can change the ionic strength of the solution. The Debye screening length and the strength of electrostatic interaction between the particle and the solid surface are thus difficult to estimate. The

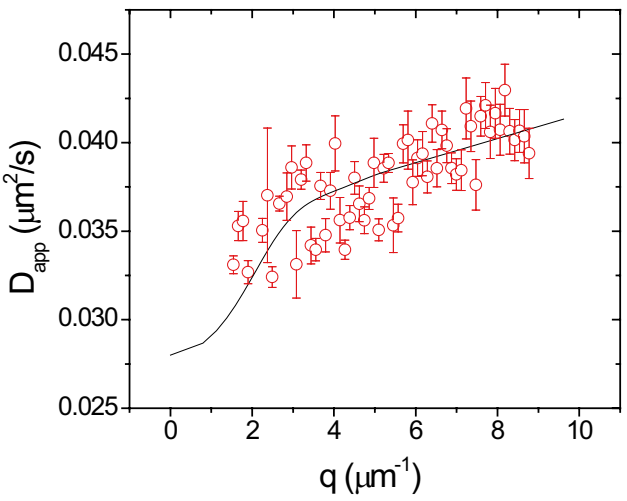

Fig. 5 The apparent diffusion coefficient, D_{app} plotted against q for surface bound particles. The solid-line fitting is with the model for thin rigid rods. The anisotropy of diffusion was ignored in this model

hydrodynamic interaction between a particle and a solid wall is a well-studied problem, both theoretically [16, 33] and experimentally [1, 27, 34]. However, a significant majority of studies focused on spherical particles undergoing translational motion. The rotational diffusion was relatively less studied, because of the paucity of tools capable of measuring rotational motion[27]. We argue that the difference in slow down of translation and rotation reflects the heterogeneous nature of surface interaction with the particles. The heterogeneity could be hydrodynamical, chemical, or topographical. One can envision a situation, where the particles are sitting atop of an ultra-thin layer of water, which can significantly quench their motion. As small changes of the thickness of ultra-confined layer can significantly alter the hydrodynamic interaction of the particles with the substrate, a dynamical heterogeneity can arise. The substrate was a microscope coverslip, which was kept overnight in a base bath and rinsed thoroughly afterwards with distilled deionized water. It removed many organic contaminants from the surface. But sub-micron scale chemical heterogeneity, which is difficult to capture by readily available methods, such as contact angle measurements cannot be ruled out. The substrates also have roughness at the scale of a nanometer, which is much small compared to the size of the particles but can be comparable to the particle surface roughness. Depending upon the contact area, it can differ from particle to particle. The very local nature of these interactions is difficult to measure experimentally. These nanoscale heterogeneities could cause inhomogeneous surface friction coefficient. Due to this, we argue that the particles experience different microenvironments, which affect translation and rotation differently. This is similar to spatially heterogeneous dynamics in supercooled liquids and glasses, which gives rise to lesser reduction of translation compared to rotation [35]. This is due to the way the motion is averaged over heterogeneities. The rotational diffusion is determined by $\langle \tau$, whereas translational diffusion is determined by $\langle 1/\tau$. Here, $\langle$.. corresponds to average over different environment. Therefore, in an ensembled average experiment, the slower particles dominate the rotational diffusion, while the faster moving particles determine the translational diffusion. Qualitatively, therefore, the heterogeneity of friction coefficient can explain the different reduction of translational and rotational diffusion of surface bound particles. The heterogeneous friction should also yield stretched exponential relaxation function. In Fig. S6, we show for surface bound particles fitting of image structure function with function of the form $\exp(-t^{\beta}/\tau)$. In all cases, we found the stretched exponent, $\beta < 1$ indicating multiple relaxation times. The deviation from $\beta = 1$, however, is small which indicates small heterogeneity and is consistent with the ensembled averaged translational and rotational diffusion data.

Conclusions

We report a quick ensemble averaged method that can determine translational and rotational diffusion of anisotropic colloids at surfaces and in bulk. For microellipsoids diffusing in deionized water, our experiments demonstrate good agreement with prediction of diffusion coefficients from Brenner theory [31]. Our results showed different reduction of translation and rotation diffusion coefficients for surface bound particle compared to their bulk values. Our method will extend the use of DDM to investigate the dynamics of anisotropic particles within complex fluids as well as expand its use to obtain their rheological and viscoelastic properties as is done in microrheology experiments. In particular, due to the local nature of rotational motion, the method can also be applied to determine friction coefficient of patterned chemically or topologically modified surfaces.

Supplementary information The online version contains supplementary material available at https://doi.org/10.1007/s00396-021-04893-8.

Acknowledgements The authors thank Prof. Michael Solomon for access to confocal set-up and useful discussion. The confocal setup is a part of the Biointerfaces Institute, University of Michigan.

Funding Acknowledgements are made to the National Science Foundation through Grant CBET-2115827.

Declarations

Competing interests The authors declare no competing of interest.

References

1. Matsuoka H, Morikawa H, Yamaoka H (1996) Rotational diffusion of ellipsoidal latex particles in dispersion as studied by depolarized dynamic light scattering. Colloids Surfaces A: Physicochem Eng Aspects 109:137–145
2. Lehner D, Lindner H, Glatter O (2000) Determination of the translational and rotational diffusion coefficients of rodlike particles using depolarized dynamic light scattering. Langmuir 16:1689–1695
3. Cush R, Dorman D, Russo PS (2004) Rotational and translational diffusion of tobacco mosaic virus in extended and globular polymer solutions. Macromolecules 37:9577–9584
4. Han Y, Alsayed AM, Nobili M, Zhang J, Lubensky TC, Yodh AG (2006) Brownian motion of an ellipsoid. Science 314:624–630
5. Tsay JM, Doose S, Weiss S (2006) Rotational and translational diffusion of peptide-coated CdSe/CdS/ZnS nanorods studied by fluorescence correlation spectroscopy. J Am Chem Soc 128:1639–1647
6. Kuipers BW, Van de Ven MC, Baars RJ, Philipse AP (2012) Simultaneous measurement of rotational and translational diffusion of anisotropic colloids with a new integrated setup for fluorescence recovery after photobleaching. J Phys Condens Matter 24:245101
7. Wilcoxon J, Schurr JM (1983) Dynamic Light scattering from thin rigid rods: anisotropy of translational diffusion of tobacco mosaic virus. Biopolymers 22:849–867
8. Alam S, Mukhopadhyay A (2014) Translational and rotational diffusions of nanorods within semidilute and entangled polymer solutions. Macromolecules 47:6919–6924
9. Anthony SM, Kim M, Granick S (2008) Translation-rotation decoupling of colloidal clusters of various symmetries. J Chem Phys 129:244701
10. Stuckert R, Plüisch CS, Wittemann A (2018) Experimental assessment and model validation on how shape determines sedimentation and diffusion of colloidal particles. Langmuir 34:13339–13351
11. Chakrabarty A, Konya A, Wang F, Selinger JV, Sun K, Wei Q-H (2013) Brownian motion of boomerang colloidal particles. Phys Rev Lett 111:160603
12. Cerbino R, Trappe V (2008) Differential dynamic microscopy: probing wave vector dependent dynamics with a microscope. Phys Rev Lett 100:188102
13. Berne BJ, Pecora R (2000) Dynamic Light Scattering New York: Dover
14. Shokeen N, Issa C, Mukhopadhyay A (2017) Comparison of nanoparticle diffusion using fluorescence correlation spectroscopy and differential dynamic microscopy within concentrated polymer solutions. Appl Phys Lett 111:263703
15. Edera P, Bergamini D, Trappe V, Giavazzi F, Cerbino R (2017) Differential dynamic microscopy microrheology of soft materials: a tracking-free determination of the frequency-dependent loss and storage moduli. Phys Rev Materials 1:073804
16. Brenner H (1961) The slow motion of a sphere through a viscous fluid towards a plane surface. Chem Eng Sci 16:242–251
17. Bayles AV, Squires TM, Helgeson ME (2016) Dark-field differential dynamic microscopy. Soft Matter 12:2440–2452
18. Reufer M, Martinez VA, Schurtenberger P, Poon WCK (2012) Differential dynamic microscopy for anisotropic colloidal dynamics. Langmuir 28:4618–4624
19. Wittmeier A, Holterhoff AL, Johnson J, Gibbs JG (2015) Rotational analysis of spherical, optically anisotropic janus particles by dynamic microscopy. Langmuir 31:10402–10410
20. Pal A, Martinez VA, Ito TH, Arlt J, Crassous JJ, Poon WCK, Schurtenberger P (2020) Anisotropic dynamics and kinetic arrest of dense colloidal ellipsoids in the presence of an external field studied by differential dynamic microscopy. Sci Adv 6:eaaw9733
21. Ho CC, Keller A, Odell JA, Ottewill RH (1993) Preparation of monodisperse ellipsoidal polystyrene particles. Colloid Polym Sci 271:469–479
22. Jaqaman K, Loerke D, Mettlen M, Kuwata H, Grinstein S, Schmid SL, Danuser G (2008) Robust single particle tracking in live cell time-lapse sequences. Nat Methods 5:695–702
23. Happel J, Brenner H (1991) Low Reynolds number hydrodynamics. Springer, Dordrecht
24. Giavazzi F, Edera P, Lu PJ, Cerbino R (2017) Image windowing mitigates edge effects in Differential Dynamic Microscopy. Eur Phys J E 40:97
25. Cerbino R, Piotti D, Buscaglia M, Giavazzi F (2018) Dark field differential dynamic microscopy enables accurate characterization of the roto-translational dynamics of bacteria and colloidal clusters. J Phys: Condens Matter 30:025901
26. Giavazzi F, Haro-Pérez C, Cerbino R (2016) Simultaneous characterization of rotational and translational diffusion of optically anisotropic particles by optical microscopy. J Phys: Condens Matter 28:195201
27. Piazza R, Degiorgio V (1996) Rotational diffusion of hard spheres: forward depolarized light-scattering measurements

and comparison to theory and simulation. J Phys: Condens Matter 8:9497–9502
28. Shimizu H (1962) Effect of molecular shape on nuclear magnetic relaxation. J Chem Phys 37:765–778
29. Tirado MM, Torre JGdl (1979) Translational friction coefficients of rigid, symmetric top macromolecules. Application to circular cylinders. J Chem Phys 71:2581–2587
30. Broersma S (1960) Viscous force constant for a closed cylinder. J Chem Phys 32:1632–1635
31. Brenner H (1974) Rheology of a dilute suspension of axisymmetric Brownian particles. Int J Multiphase Flow 1:195–341
32. Vasanthi R, Bhattacharyya S, Bagchi B (2001) Anisotropic diffusion of spheroids in liquids: slow orientational relaxation of the oblates. J Chem Phys 116
33. Cichocki B, Jones RB (1998) Image representation of a spherical particle near a hard wall. Phys A 273:273–302
34. Rogers SA, Lisicki M, Cichocki B, Dhont JKG, Lang PR (2012) Rotational diffusion of spherical colloids close to a wall. Phys Rev Lett 109:098305
35. Cicerone MT, Ediger MD (1996) Enhanced translation of probe molecules in supercooled o-terphenyl: signature of spatially heterogeneous dynamics? J Chem Phys 104:7210–7218